An Analysis of Inertial Oscillations Observed Near Oregon Coast

PIJUSH K. KUNDU[1]

School of Oceanography, Oregon State University, Corvallis 97331

(Manuscript received 15 March 1976, in revised form 23 July 1976)

ABSTRACT

Nearly two months of current meter data taken during the summer of 1973 at eleven depths at a station off the coast of Oregon in 100 m of water have been analyzed. The spectra show an 8% increase in the frequency of the inertial peak ($\omega \approx 0.064$ cph) above the local f ($=0.059$ cph). Because of the close proximity of the tidal frequencies to the local f, a sharp bandpass filter centered at $\omega = 0.064$ cph was used to isolate the inertial motions. The results showed that the amplitude of the inertial oscillations decayed slowly with depth, but the decay within about 10 m of the bottom was more rapid. A lagged correlation of the inertial currents clearly showed an upward propagation of phases throughout the water column, at a speed of about 0.1 cm s^{-1} within the depth range 20–60 m, but generally higher both above and below this mid-depth. The inertial currents were found to turn clockwise (looking down) with depth, which corresponds to an upward phase and downward energy propagation, and the vertical phase speeds implied by the rates of turning agreed remarkably well with the lagged correlation calculations. The vertical wavelength was found to be of the order of the water depth. The vertical flux of energy into the bottom boundary layer during the occurrence of inertial bursts was estimated to be of the same order as the rate of turbulence production within the boundary layer, signifying that the inertial bursts can cause appreciable boundary layer stirring. The average hodographs of the horizontal velocity vectors were found to be ellipses of axis ratio 1.03–1.28; a majority of them had their major axes aligned roughly perpendicular to the coast, signifying propagation in that direction. It was found that the simple wind-forced model of Pollard and Millard does qualitatively reproduce many of the observed features of the inertial currents in the surface layer.

1. Introduction

Oscillations with a frequency close to the local inertial frequency f are observed in the ocean and large lakes at all depths. The important characteristics observed are:

1) The horizontal velocity vector rotates clockwise (Northern Hemisphere) with time with nearly but not exactly constant speed. The maximum speeds observed are about 10–20 cm s^{-1}.

2) The observed frequency ω is generally slightly (3%–20%) above f (Day and Webster, 1965; Gonella, 1971; Perkins, 1972; Fomin, 1973; Leaman, 1975).

3) There is a correspondence between the passage of storms and inertial oscillations in the surface layer (Pollard and Millard, 1970; Gonella, 1971; Halpern, 1974).

4) The oscillations are highly intermittent and last only a few oscillations (Webster, 1968; Tomczak, 1968). This can be caused by a large frequency spread of the near-inertial oscillations (Munk and Phillips, 1968).

5) Vertical coherence scales are of the order of only a few tens of meters (Webster, 1968; Halpern, 1974; Fomin and Savin, 1973), whereas the horizontal coherence scale is of the order of a few tens of kilometers (Webster, 1968; Schott, 1971).

6) An exception to 4) and 5) is the work of Perkins (1970, 1972) in the Mediterranean, which showed a long persistence of about two weeks, a low-frequency spread, and a large vertical coherence scale of more than 1 km. Perkins (private communication) believes that this may be a general property of enclosed seas.

7) There is evidence of an upward propagation of phase. The depth profiling current meter measurements of Johnson *et al.* (1976), and to some extent of Leaman (1975), provide a striking visual evidence of this fact. The measurements of Johnson *et al.* were conducted in 100 m of water near the coast of Oregon (Fig. 1). From their measurements (reproduced in Fig. 2 here) the vertical phase speed is estimated to be about 0.1 cm s^{-1} ($\sim$86 m day^{-1}), which seems to be almost constant throughout the middle depths of 25–70 m. The period seems to be about 16 h, and the vertical wavelength about 50 m, making the phase speed estimate consistent with the relation speed = length/period. Leaman's measurements were conducted in 5500 m of water near Bermuda. He estimates phase speeds of 0.2 cm s^{-1} at 500 m and 0.6 cm s^{-1} at 2000 m.

8) Downward propagation of wave packets is also strikingly displayed in the eastward velocity contours

[1] Present affiliation: Instituto Oceanografico, Universidad de Oriente, Cumaná, Venezuela.

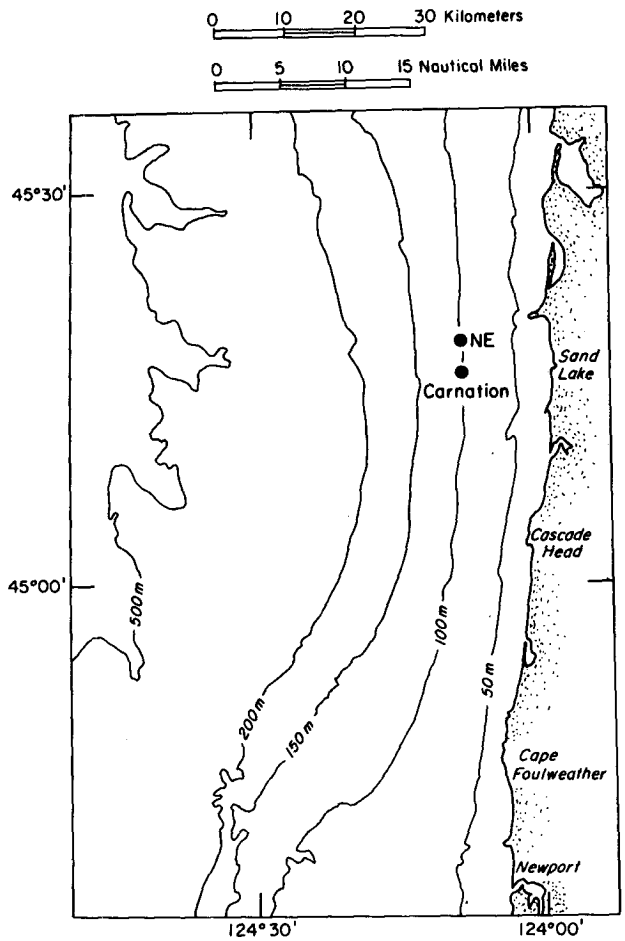

FIG. 1. Location of current meter station Carnation. Isobaths are in meters. The location of the cyclesonde experiment of Johnson *et al.* (1976) is indicated by NE.

of Fig. 2, from which the vertical group velocity is estimated to be about 0.03 cm s^{-1}, and this speed seems to be approximately constant throughout most of the water column. Frankignoul (1974) gave a much higher downward speed of energy propagation of 0.5 cm s^{-1}, but he (private communication) no longer accepts this value.

In this work, some characteristics of the inertial waves will be determined from current meter data taken in the surface as well as in the deeper layers at a station near the coast of Oregon. Much of these data were also used in the work of Hayes and Halpern (1976), who studied the entire internal wave range of frequencies by computing the time series of Fourier coefficients of short segments of data. For the inertial frequency band, they found that the bursts of energy at all depths in the mixed layer (~20 m thick) occur almost simultaneously, with the energy decaying rapidly in depth. In this work, we shall isolate the inertial motions by using a band-pass filter which passes energy only in a narrow frequency interval around the inertial peak. A frequency shift of the inertial peak, an upward phase movement, and a clockwise turning of currents with depth will be established, and many other parameters of the wave field will be estimated.

The other aim of the present work is to apply the model of Pollard and Millard (1970) for inertial wave generation in the surface layer. These authors have found a surprisingly good resemblance between an extremely simple model of forcing by a wind stress, and the surface current data taken at "site D" of the Woods Hole Oceanographic Institution. The success of this very simple model is intriguing, and it is important that their procedure be repeated in an independent work. One purpose of the present paper is to compare the results of the Pollard-Millard model with the surface current meter data taken near the Oregon coast. It will be found that the model can reproduce many of the observed inertial currents in a qualitative way.

2. The data base

The data are part of the Coastal Upwelling Experiment (CUE-2) conducted in the summer of 1973 near the coast of Oregon. Nearly two months of current meter data at eleven depths at a station named Carnation (water depth 100 m) will be studied (Fig. 1). The measurements at depths of 3.4 m, 7.7 m, 9.9 m, 14.3 m, 16.3 m and 18.3 m were taken on a surface mooring deployed by the Pacific Marine Environmental Laboratory, and are described in Halpern *et al.* (1974a). The measurements at depths of 20.2 m, 40.4 m, 60.6

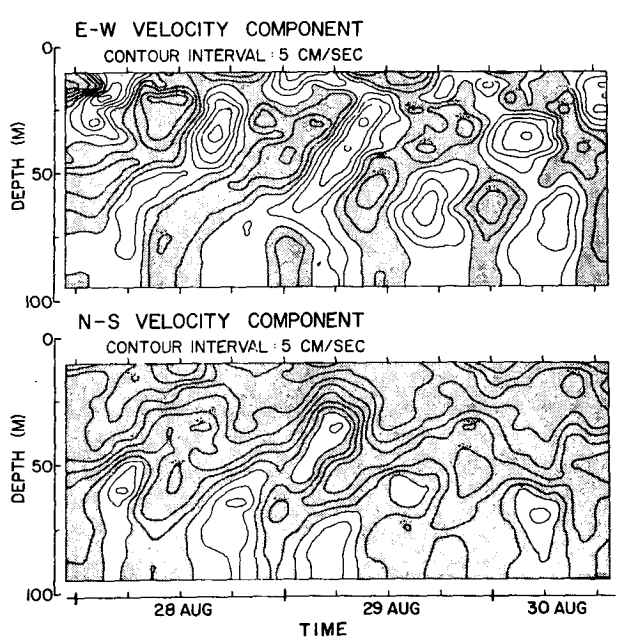

FIG. 2. Time-depth contours of the velocity components in the cyclesonde measurements of Johnson *et al.* (1976) from which this figure is reproduced. The westward and southward velocities are shaded.

m, 80.8 m and 95.9 m were taken on a subsurface mooring by Oregon State University, and are described in Pillsbury *et al.* (1974). The wind data used were measured at the coast at Newport; those measured on the surface buoy at Carnation were very similar.

From the 15 or 10 min observations, hourly series were first formed after removing the higher frequencies by means of a low-pass filter having a half-power point of 0.5 cycles per hour (cph).

The density field in this region changes rapidly in time because of the occurrence of the coastal upwelling phenomenon (Hayes and Halpern, 1976). Fig. 3 shows the average vertical distribution of the Brunt-Väisälä frequency N during the duration of the experiment, computed from the hydrographic measurements made from an anchor station at Carnation.

Before studying the data, a brief resume of the theoretical relations needed will be given.

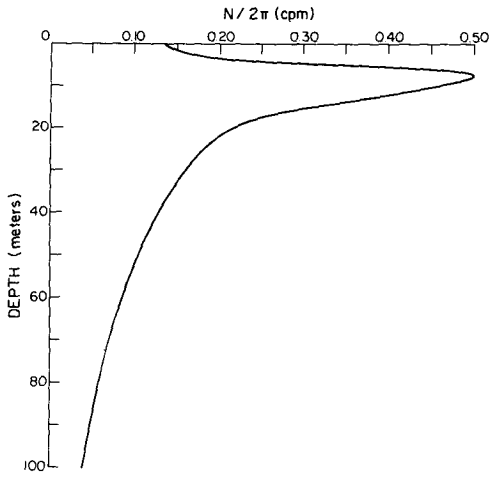

FIG. 3. Vertical distribution of Brunt-Väisälä frequency $N(z)$, averaged over 193 hydrographic profiles taken during the duration of the current meter experiment (reproduced from Kundu *et al.*, 1975).

3. The WKB solution of inertial-internal waves

The approximate WKB solution of the linear inertial-internal wave equations for slow variations of the Brunt-Väisälä frequency $N(z)$ are well known, and many of these results will be used in this work. An outline of the solution will first be described, since a simple presentation of these relations is not readily found in the literature. [But see, e.g., Leaman (1975)]. The horizontal scales of the wave field will be assumed sufficiently small so that β effects [e.g., Munk and Phillips (1968); Kroll (1975)] are unimportant for a local description.

Neglecting the effects of mean shear and horizontal density gradients, the nondiffusive linearized equations of motion are

$$u_x+v_y+w_z=0, \tag{3.1}$$

$$u_t-fv=-p_x/\rho_0, \tag{3.2}$$

$$v_t+fu=-p_y/\rho_0, \tag{3.3}$$

$$w_t=-p_z/\rho_0-\rho g/\rho_0, \tag{3.4}$$

$$\rho_t-w\rho_0N^2/g=0, \tag{3.5}$$

where the symbols have their usual meaning. The coordinates are x (eastward), y (northward), and z (upward).

Eqs. (3.1)–(3.5) can be combined into

$$\nabla^2w_{tt}+N^2\nabla_H{}^2w+f^2w_{zz}=0, \tag{3.6}$$

where ∇^2 is the three-dimensional and $\nabla_H{}^2$ the horizontal Laplacian. Assuming solutions of the form

$$w=\hat{w}(z)\exp i(kx+ly-\omega t), \tag{3.7}$$

Eq. (3.6) gives

$$\hat{w}_{zz}+m^2\hat{w}=0, \tag{3.8}$$

where

$$m^2(z)=(k^2+l^2)\frac{N^2(z)-\omega^2}{\omega^2-f^2}. \tag{3.9}$$

Note that m is real for the inertial-internal frequency range $f<\omega<N$.

If the scales of variations of $N(z)$ are larger than the vertical scales of the motion then $N(z)$, and hence $m(z)$, can be regarded as slowly varying functions of z. This is a good approximation when the vertical mode numbers are high, which does not appear to be true in the present study. We shall, however, use these relations and hope that they do provide order of magnitude estimates. Asymptotic WKB solutions can then be obtained for (3.8). In the lowest order, the two possible solutions (see, for example, Nayfeh, 1973, p. 318) are

$$\hat{w}=Am^{-\frac{1}{2}}\exp\left(\pm i\int^z m\,dz\right), \tag{3.10}$$

where A is an arbitrary constant. The corresponding vertical distributions of u and v can be obtained from (3.1)–(3.3):

$$\hat{u}=\mp A(\omega k+ifl)\frac{m^{\frac{1}{2}}}{\omega(k^2+l^2)}\exp\left(\pm i\int^z m\,dz\right), \tag{3.11}$$

$$\hat{v}=\pm A(ikf-\omega l)\frac{m^{\frac{1}{2}}}{\omega(k^2+l^2)}\exp\left(\pm i\int^z m\,dz\right). \tag{3.12}$$

Assume that the x-axis is now oriented in the direction of horizontal propagation, so that $l=0$. Eqs. (3.11) and (3.12) then give, taking real part,

$$u=\mp A\frac{m^{\frac{1}{2}}}{k}\cos\left(kx\pm\int^z m\,dz-\omega t\right), \tag{3.13}$$

$$v=\mp A\frac{f}{\omega}\frac{m^{\frac{1}{2}}}{k}\sin\left(kx\pm\int^z m\,dz-\omega t\right). \tag{3.14}$$

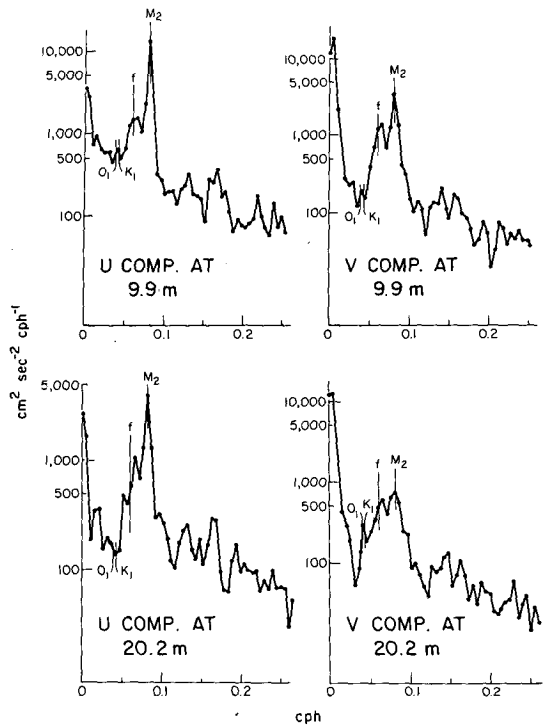

FIG. 4. Some typical spectra of u and v components. Bandwidth =0.005 cph. Note the shift of the inertial peak.

These show that $\partial(\text{phase})/\partial z = m(z)$, so that $m(z)$ is a local vertical wavenumber. In these equations k, m, $\omega > 0$, and the upper signs represent upward propagating waves while the lower signs represent downward propagating waves. Since $N(z) \gg \omega$ for the case in hand, the foregoing equations show that the z-dependence is given by $m \propto N$, $w \propto N^{-1}$ and u, $v \propto N^{1}$, assuming ω is independent of z.

Eqs. (3.13) and (3.14) show that the horizontal velocity vector at any fixed point in space describes a clockwise ellipse as a function of time; the major axis is aligned with the horizontal direction of propagation and the ratio of major to minor axis is ω/f. However, there is also a turning of the horizontal velocity vector as a function of z. In fact, the tip of the velocity vector at a given time describes a helix having its axis aligned with the direction of propagation (Leaman and Sanford, 1975). The sense of polarization is *clockwise* (looking down) with increasing depth if the phases are propagating *up*, and counterclockwise if the phases are propagating down.

The dispersion relation is (3.9). It is easy to show that, for $N > f$, the phase and group velocity vectors are at right angles, and their vertical components have opposite signs. From the dispersion relation (3.9), the vertical component of the group velocity is

$$c_g = \frac{\partial \omega}{\partial m} = \frac{(f^2-\omega^2)(N^2-\omega^2)}{m\omega(N^2-f^2)} \approx c[(f/\omega)^2-1], \quad (3.15)$$

where $c = \omega/m$ is the vertical component of the phase speed.

So far the effects of the mean shear and horizontal density gradients have been neglected. This may not be a valid assumption in the upwelling region under study, which is characterized by large shears. Mooers (1975) has considered this problem theoretically, and among other things has shown that for cross-stream propagation all propagation properties are altered, including the passband for internal-inertial waves:

$$(f^2 + f\bar{v}_x - s^2N^2)^{\frac{1}{2}} \lesssim \omega \lesssim N(1+s^2)^{\frac{1}{2}}, \quad (3.16)$$

where s is the slope of the isopycnals and $\bar{v}_x$ is the mean horizontal shear.

4. Shift in inertial peak

It has been stated before that there is considerable evidence indicating that the "inertial" peak actually occurs at a frequency somewhat larger than the local f. By "inertial" motions one usually refers to these near-inertial oscillations.

It is evident from the last section that $\omega > f$ for internal wave motions. As $\omega \to f$, the phase velocity vector becomes increasingly vertical and the group velocity vector becomes increasingly horizontal, vertical component of both vanishing at $\omega = f$. However, the process of generation (in the surface layer by the wind, and possibly in the bottom layer by the topographic roughness) and propagation have to be accounted for in the behavior of the inertial motions in the real ocean, which would require $\omega > f$. It is important to see if the spectra of the currents show such a shift of the inertial peak.

The spectra of u and v of all current series were computed using 13–14 degrees of freedom and a bandwidth of 0.005 cph. All of them displayed two main peaks: semidiurnal and inertial; the diurnal peak was smaller. Four typical spectra are shown in Fig. 4. The bandwidth of the inertial peak is seen to be fairly large, the peak being rather unlike the thin and sharp tidal peaks. It is this fact which causes small persistence (intermittency) of the inertial oscillations (Munk and Phillips, 1968), since persistence is of the order of the reciprocal of the bandwidth. [This can be easily seen by considering the case of the sum of two series of nearly equal frequencies: $\cos 2\pi\omega_1 t + \cos 2\pi\omega_2 t = 2\cos\pi(\omega_1+\omega_2)t \cos\pi(\omega_1-\omega_2)t$, where the modulation envelope $\cos\pi(\omega_1-\omega_2)t$ has a lobe width $T = (\omega_1-\omega_2)^{-1}$.] From Fig. 4, the inertial bandwidth is estimated to be about five times the basic bandwidth of the spectral estimates, i.e. 0.025 cph, giving a persistence of 40 h, or about $2\frac{1}{2}$ inertial periods.

However, Fig. 4 shows that the maximum of this broad peak occurs at a frequency slightly larger than f(=0.592 cph). In order to find the location of the inertial peak more accurately, higher resolution spectra of all the currents were computed near the inertial fre-

quency, using a bandwidth of 0.002 cph and slightly more than 5 degrees of freedom. Out of the eleven current series, six were found to peak at 0.064 cph, three (namely at 3.4 m, 80.8 m and 95.9 m) at 0.066 cph and two (namely at 40.4 m and 60.6 m) at 0.062 cph. The peaks of u and v occurred at the same frequency. Many of them showed a smaller secondary peak at 0.058 cph; there was no specific depth range at which this behavior was observed. Fig. 5 shows the arithmetic average of all the eleven kinetic energy spectra at the station. It is seen that, although there is a smaller secondary peak at about 0.058 cph, the main inertial peak is at 0.064 cph (period $\sim$15.6 h), giving rise to a frequency shift of about 8% above f.

Evidence of the shift in the location of the inertial peak was also found by complex demodulating the series at $\omega=0.064$ cph, which showed that the phase of the motion does not appreciably change with time during the main bursts of amplitude, signifying that the motions during these large bursts have a frequency near 0.064 cph.

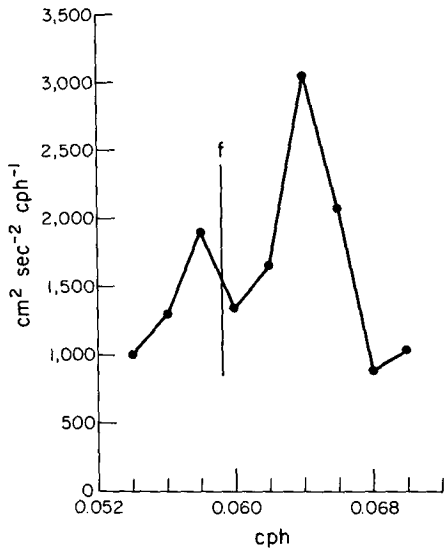

FIG. 5. High-resolution spectra of KE ($=u^2+v^2$), averaged over all eleven depths. Bandwidth=0.002 cph. Note the shift of the inertial peak to 0.064 cph, and the secondary peak at 0.058 cph.

5. Application of Pollard-Millard model

Pollard and Millard (1970) obtained a good correlation between the observed inertial currents in the surface layer at site "D" and a computed current based on a very simple model of wind forcing. The model currents in the mixed layer were computed according to

$$\frac{\partial u}{\partial t}-fv=\frac{\tau_x}{\rho a}-cu, \tag{5.1}$$

$$\frac{\partial v}{\partial t}+fu=\frac{\tau_y}{\rho a}-cv, \tag{5.2}$$

where $\boldsymbol{\tau}=(\tau_x,\tau_y)$ is the wind stress, ρ is the water density, a is the mixed layer depth, and c^{-1} is the e-folding decay time which models the dispersion effect by introducing a decay factor of the form $\exp(-ct)$.

The stresses in (5.1)–(5.2) were computed from $\boldsymbol{\tau}=c_D\rho_a|\mathbf{V}|\mathbf{V}$, where $\mathbf{V}$ is the hourly wind velocity; the density of the air is taken as $\rho_a=1.22\times10^{-3}$ g cm^{-3}, and $c_D=1.4\times10^{-3}$. The magnitude of the depth of the mixed layer, whose effect was essentially to control the amplitude of the model current, was varied between 10 and 25 m, and c^{-1} was varied between 2 days and 8 days. Assuming zero initial conditions (5.1) and (5.2) were integrated forward in time using a Runge-Kutta scheme and a time step of 1 h, yielding time series for u and v. (A different initial condition, namely setting the model initial current to be equal to the observed current in the mixed layer, was also tried. The effect of this difference in the initial condition, however, vanished after the first few days, because of the presence of the decay factor.)

The amplitude and phase of the inertial components of the model and observed currents were then determined by demodulating at frequency f. A modified version of the technique of complex demodulation of a two-dimensional series, as developed by Perkins (1970) and used by Pollard and Millard (1970), was used. Let $\mathbf{U}(t)=u+iv$ be the vector series. One is interested in a complex coefficient $\mathbf{D}(\tau)$ so that the idealized inertial wave $\mathbf{D}\exp(-ift)$ most closely resembles $\mathbf{U}$ in a specified interval of time $2T$ centered around τ. A variational argument quickly shows (Perkins, 1970) that

$$\mathbf{D}(\tau)=\frac{1}{2T}\int_{\tau-T}^{\tau+T}e^{ift}\mathbf{U}(t)dt. \tag{5.3}$$

The magnitude and argument of the complex number $\mathbf{D}$ gives the amplitude and phase of the inertial motion at time τ. The above formulation obviously results in a $(\sin x)/x$ form of spectral window which is not suitable in the present case because of the close proximity of strong tides on the two sides of the inertial peak. Eq. (5.3) was therefore modified as

$$\mathbf{D}(\tau)=\frac{1}{2T}\int_{\tau-T}^{\tau+T}e^{ift}W(t)\mathbf{U}(t)dt, \tag{5.4}$$

where the filter $W(t)$ has a sharp response characteristic shown by the dotted curve in Fig. 6, and $2T$ is the length of the filter. The technique used in Perkins (1970) was slightly different in that no such filter was necessary because his Mediterranean data were almost free of tides, and an actual least squares technique was used instead of a straightforward application of (5.3).

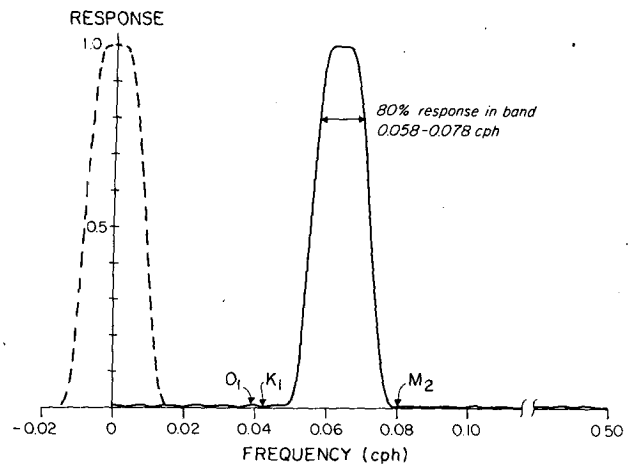

FIG. 6. Response of filters. The dotted curve shows the low-pass filter used in demodulation, and the continuous curve shows the bandpass filter (centered at 0.064 cph) used to separate the inertial motions. The two filters have the same shape, displaced in frequency only.

The method of complex demodulation, whether applied on a scalar or a two-dimensional series like ours, would provide information on the variation of the amplitude and phase of a particular frequency (strictly, a frequency "band"), if the component of motion at this frequency changes *slowly* with time, so that it does not change much during a time interval equal to the effective length of the filter. Otherwise, a spreading or smearing of the energy in the time domain results. The total length of the filter used was 223 hours (~9 days), but some experiments with it showed that the spreading occurs only over about 4 days, since the two tails of the filter are rather light and do not cause much spreading. However, even a filter of 4 days effective width is expected to cause time-smearing, since inertial motions are highly intermittent and exist only a few cycles. It was, however, decided to accept this, since the other alternative of applying no filter would cause inclusion of part of the tidal energy.

Complex demodulation of a scalar series without the application of a filter is equivalent to computing raw Fourier coefficients of short segments, as used, for example, in Hayes and Halpern (1976). Our estimate shows that the resulting $(\sin x)/x$ form of spectral window caused an admission of 15% of the amplitude of the M_2 tide, 1% of the K_1 tide, and 12% of the O_1 tide in their work. The admission of this fair amount of M_2 tide would cause appreciable error, since the semidiurnal amplitudes are typically 2–3 times the inertial amplitudes (Fig. 4). Also, not all of the inertial energy was admitted because the 8% frequency shift of the inertial peak was not detected.

The amplitude and phase of the complex series of $\mathbf{D}(\tau)$ were computed for the model current, as well as for the observed currents in the mixed layer at depths of 3.4 m, 7.7 m, 9.9 m and 14.3 m. If the parameters a and c were properly chosen, then some qualitative similarities were noticed. One typical example is shown in Fig. 7, which compares the model current with the 7.7 m current. (The amplitude and phase of the observed currents at other depths of the mixed layer were quite similar to those at 7.7 m.) The numerical values used in this computation were $c^{-1}=2$ days and $a=15$ m, the latter value being in agreement with the observed mixed layer depth of 10–20 m during the duration of the experiment (Halpern, 1976). The observed and model currents are seen to have large amplitudes during 10–13 July, 27 July–3 August and 14–18 August. However, the large observed amplitudes during 21–23 July are totally absent in the model since the local wind was very weak. This means that not all the inertial currents in the mixed layer can be traced back to the local wind forcing or to the model.

The predominance of a "linear" decrease of the observed phase can be seen throughout most of the record. The increase of the phase during 13–19 July is not significant since the amplitude was low, and the only period during which the observed phase significantly increased was during 12–16 August. The dominance of a linear decrease of phase suggests that the actual frequency was larger than the demodulation frequency f. From the slope of the phase ϕ, one gets $\Delta\omega=\Delta\phi/\Delta t=0.005$ cph, giving the actual frequency to be $f+\Delta\omega\approx 0.064$ cph, consistent with the spectral calculation presented in the last section.

The increasing observed phase during 12–16 August suggests the presence of frequencies smaller than f during certain time intervals. A careful counting of the period of the bandpass filtered inertial time series

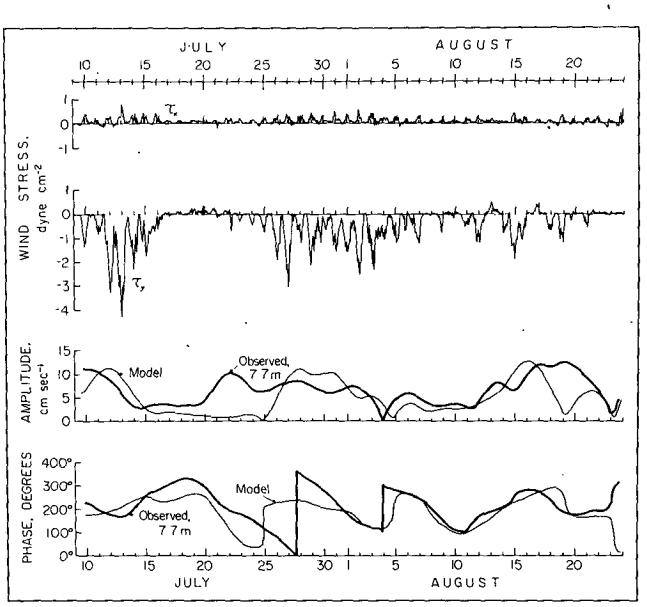

FIG. 7. Comparison of the amplitude and phase of the inertial current in the mixed layer at 7.7 m with the one obtained from the Pollard-Millard model. The amplitude and phase were obtained by demodulating at f.

(Fig. 10, explained in the next section) showed that the frequency during the event of 12–16 August at 7.7 m was indeed slightly less than f. The conclusion, therefore, is that the events predominantly have a frequency of about 8% above f, but some individual events had frequencies close to or even less than f.

A comparison of the phases of the model and observed currents suggests an excellent agreement. A close scrutiny, however, reveals that the agreement appears better than it really is. For example, the similarities during 15–25 July and 5–10 August are not significant since the model current was of small magnitude during these periods.

The model current does not show the dominant decreasing trends that is a feature of the observed current, since its frequency is not expected to be slightly larger than f. It is easy to show that the system (5.1)–(5.2) has a free solution of the form $\exp(ift)$, whereas the forced solution is maximum at a forcing frequency of $(f^2-c^2)^{\frac{1}{2}}$, that is, at a frequency slightly less than f (Pollard and Millard, 1970). For our assumed value of $c^{-1}=2$ days, the frequency $(f^2-c^2)^{\frac{1}{2}}$ is 0.16% *below* f. The model currents could not, therefore, have a frequency slightly *greater* than f, as observed frequently, unless the spectrum of the wind stress itself was peaked at a frequency somewhat larger than f. A spectrum analysis of the wind stress showed that that was not the case. It is therefore expected that the trends of the model and phase spectra should not be very similar. In any case, the agreement in the phases of the model and observed currents is fairly convincing.

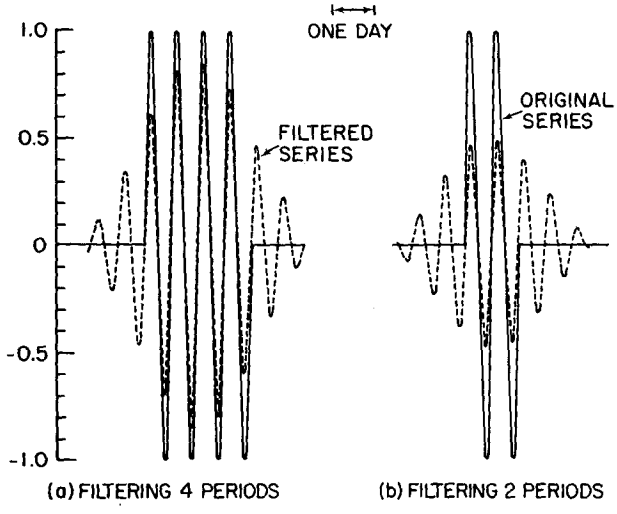

FIG. 8. The effect of band-pass filtering a few cycles of the inertial event. (a) The original series consisting of 4 cycles, and zeros elsewhere. (b) The original series consisting of 2 cycles, and zeros elsewhere. Note that the filtering process spreads the event by about 4 days, cuts down the maximum value, but does not alter the phase.

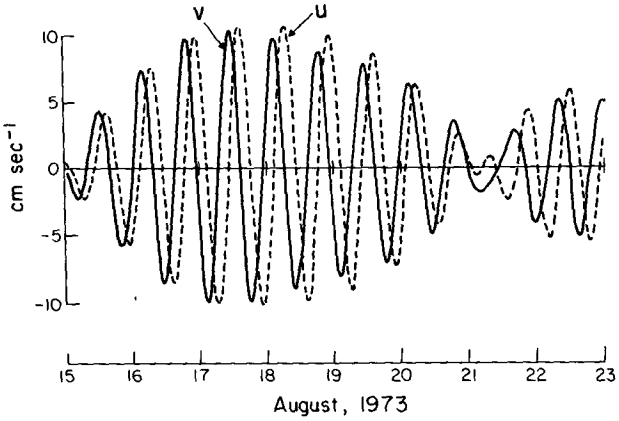

FIG. 9. Eastward and northward components of the band-pass filtered current at 7.7 m during 15–23 August. Note the almost equal magnitude of u and v, and the approximate 90° lag of u behind v.

6. Band-pass filtering the data

In order to extract the inertial contents of the data series, a bandpass filter was used. The method of bandpass filtering at inertial frequency also used by Tomczak (1968). The frequency response of the filter used is shown by the continuous curve in Fig. 6. It has the same shape as the one used in the demodulation, but is centered at $\omega=0.064$ cpd. Note that the response at tidal frequencies is practically zero.

The smearing of peaks due to sharp filtering was tested on a few synthetic time series resembling intermittent inertial motions of a few cycles of 0.064 cph. The rest of the series was made up of zeros. The effect of applying the bandpass filter on such series is shown in Fig. 8, where it is seen that the filtering process smears the original series over a length of about 4 days. The smearing is more pronounced if the number of cycles in the original series is low. For example, Fig. 8 shows that the maximum is reduced to about 50% of its original magnitude if the original event consists of 2 cycles, whereas it is about 80% if the event consisted of 4 cycles. [Fig. 2 shows that the inertial event of Johnson *et al.* (1976) consisted of about 2 cycles.]

The symmetric filter used does not alter the phases of the original series, a fact which permits using them in the calculations of the following sections.

The u and v components of all the currents were band-pass filtered. A segment of the filtered u and v series at 7.7 m is shown in Fig. 9. Note that u and v are very nearly equal, and that u lags v by about 90°, signifying that the currents are indeed nearly circularly polarized and rotating clockwise. All the filtered u series are displayed in Fig. 10. The v series are not shown to avoid overcrowding, but most of the time they were about the same amplitude as u but led by approximately 90°. Although a typical maximum magnitude of the inertial current shown in Fig. 10 is about 10–13 cm s^{-1}, the real maximum before peak smearing

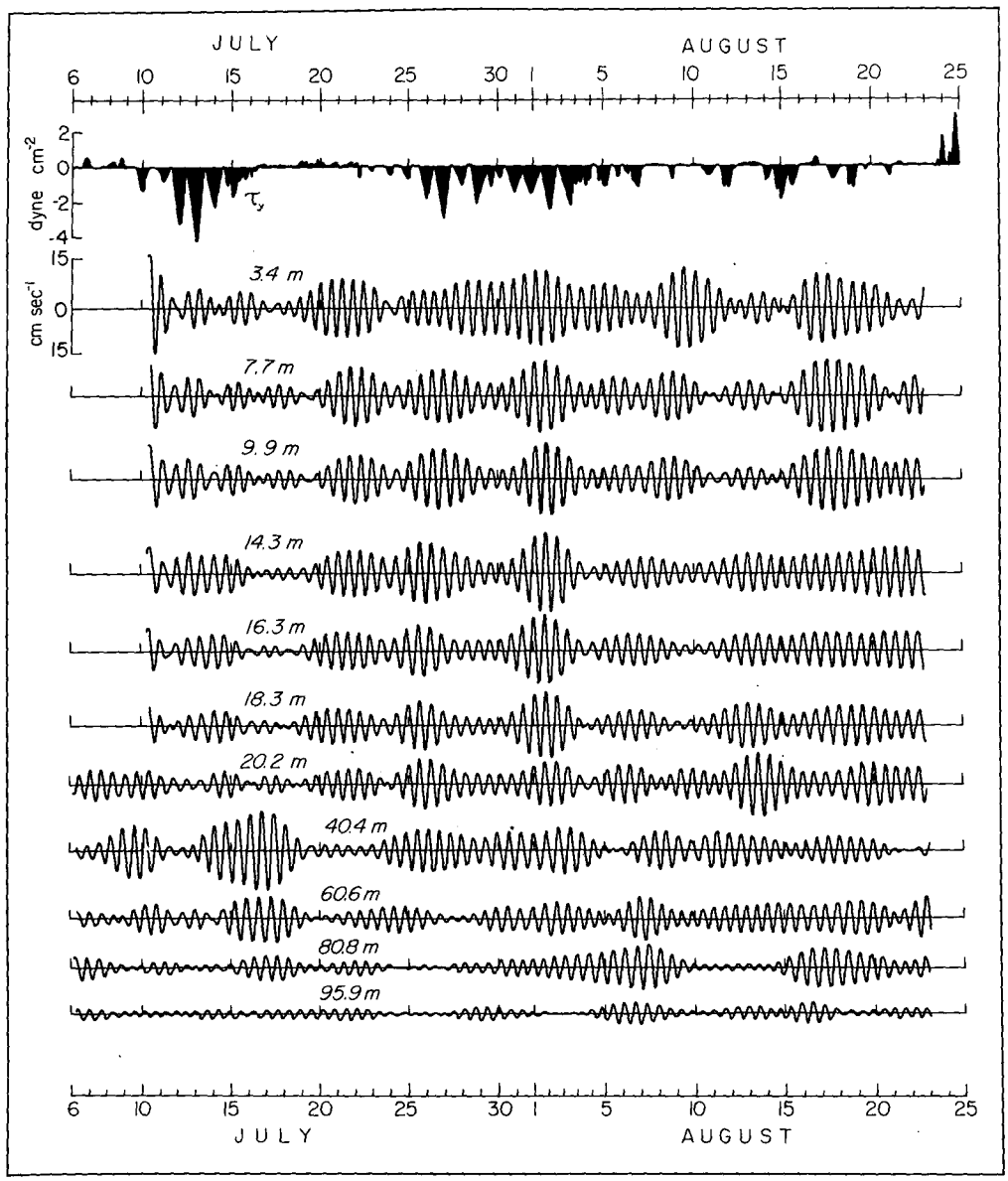

FIG. 10. Eastward component of the band-pass filtered current at all depths.

would have been 20–25 cm s^{-1}, if the inertial event consisted of 2 cycles.

The peaks and valleys of the currents in the top 20 m can be seen to occur approximately simultaneously. However, a close examination showed that the oscillations were slightly leading in the deeper layers, signifying an upward propagation of phase (see Section 8 for details).

The filtered u and v series were used for further calculations. In all of the following computations, the data within the upper 40 m during the time period 1 August–9 August were discarded, since the behavior of the filtered data during that period was rather unlike near-inertial waves, having a large u and a small v nearly in phase with it, suggesting approximately rectilinear motion at a small angle with the east-west direction.

7. Shape of average inertial hodograph

It has been pointed out in Section 3 that the horizontal hodographs of all the internal waves are clockwise ellipses, the major axes of which are oriented along the direction of phase propagation, the axis ratio being ω/f. The hodographs of near-inertial waves are therefore nearly circular. It will be shown that the behavior of the band-pass filtered series is not inconsistent with this picture.

Table 1 shows the relevant quantities for computing the size and orientation of the average hodograph

TABLE 1. Results of hodograph ellipse calculations for inertial currents.

Depth (m)	$\sqrt{\overline{u^2}}$ (cm s^{-1})	$\sqrt{\overline{v^2}}$ (cm s^{-1})	$\frac{\overline{uv}}{(\overline{u^2}\,\overline{v^2})^{\frac{1}{2}}}$	θ (degrees, clockwise from east)	A (cm s^{-1})	B (cm s^{-1})	$\frac{A}{B}$
3.4	4.56	4.24	0.04	15°	6.48	5.95	1.09
7.7	4.21	3.98	0.02	9°	5.97	5.61	1.06
9.9	3.74	3.90	0.01	81°	5.53	5.28	1.05
14.3	3.78	3.30	0.04	8°	5.36	4.65	1.15
16.3	2.96	2.61	0.07	15°	4.21	3.65	1.15
18.3	2.89	2.50	0.13	21°	4.19	3.44	1.21
20.2	3.06	2.75	0.12	3°	4.37	3.87	1.13
40.4	3.43	2.83	0.23	25°	4.95	3.87	1.28
60.6	2.50	2.69	−0.04	−74°	3.73	3.61	1.04
80.8	2.03	1.87	0.14	29°	3.04	2.46	1.24
95.9	0.98	0.88	−0.05	−12°	1.44	1.17	1.23

ellipses at various depths. The band-pass filtered series at $\omega=0.064$ cph were used. The nonzero values of $\overline{uv}$ (the overbar denotes time average) in Table 1 show that u and v are not exactly 90° apart in the east-north coordinate system. The major axis orientation was computed from

$$\theta=\tfrac{1}{2}\tan^{-1}\frac{2\overline{uv}}{\overline{u^2}-\overline{v^2}}, \tag{7.1}$$

while the lengths of the major (A) and minor (B) axes were determined from

$$A^2,\ B^2=\overline{u^2}+\overline{v^2}\pm[(\overline{u^2}-\overline{v^2})^2+4\overline{uv}^2]^{\frac{1}{2}}. \tag{7.2}$$

The time-averaged size of the hodographs, represented by A or B, appears to be about 6 cm s^{-1} in the upper layers. This is much smaller than the maximum velocities of about 20 cm s^{-1}, because of the intermittent nature of the inertial motion. The smearing phenomenon acts on u and v components in a similar manner, and it is expected that the axes ratio A/B and the ellipse orientation θ are not affected very much.

The ratio A/B varies between 1.04 and 1.28, which is consistent with the ideal value of 1.08 at $\omega=0.064$ cph. The direction of propagation, given by the orientation of the major axis (θ) of the ellipses, is generally aligned approximately east-west. The only two exceptions are at 9.9 m and 60.6 m where the direction is seen to be roughly north-south, but the orientation in these two cases is less reliable because A/B is very close to unity (1.04–1.05).

Table 1 also shows that the amplitude of the inertial motion decays slowly with depth. At a depth of 80 m, its average magnitude is about half of that in the surface layer. Within the bottom frictional layer, the 95 m data show a rapid decay of inertial oscillations, although the very low frequency "geostrophic" velocity drops by only about 15% between 80 and 95 m (Kundu, 1976). The monotonic decrease of the rms velocities between 10 and 80 m is in fair agreement with the WKB solution $u, v\sim N^{\frac{1}{2}}$. Fig. 3 shows that the maximum of N occurs at a depth of about 10 m, and a monotonic decrease thereafter. Obviously, the observed behavior of the rms velocities above 10 m does not follow the WKB scheme, which is not surprising since the theory only treats the propagation and not the generation process in the mixed layer. Between 10 and 80 m depths, $N^{\frac{1}{2}}$ decreases by a factor of about 2.7, whereas the rms speeds fall by a factor of about 2, showing qualitative agreement in this region. Leaman and Sanford (1975) found a similar agreement.

8. Vertical phase propagation

The recent depth-profiling current meter data of Leaman (1975) and Johnson *et al.* (1976) have clearly demonstrated an upward phase propagation throughout a major part of the water column. Although the dominant period in these fluctuations indeed seems inertial, other frequencies were definitely present. In this section the existence of the vertical phase propagation of the inertial waves will be investigated by finding the lagged correlation of the band-pass filtered u components. Note that the symmetric filter used caused a smearing of the peaks in the time domain, but did not change their phases.

A visual inspection of the currents in the original large format version of Fig. 10 clearly showed an *upward* propagation of phase. The small phase shift with depth is not visible in the smaller reproduction of this figure. The magnitude of the phase speed was found by computing the lagged cross correlation function between currents at two depths 1 and 2 according to

$$R(\tau)=\frac{\overline{u_1(t)u_2(t-\tau)}}{(\overline{u_1^2}\,\overline{u_2^2})^{\frac{1}{2}}}. \tag{8.1}$$

The maximum correlation was found to be negligibly small for currents separated by more than 20 m. A few

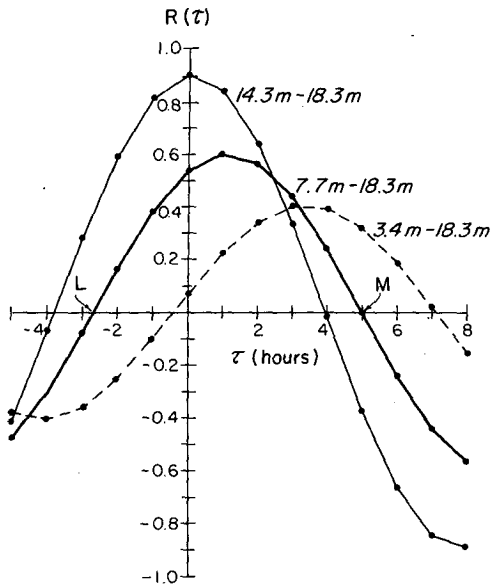

FIG. 11. Some typical cross correlation functions. A maximum at a positive lag corresponds to the second series leading the first. For the 7.7 m–18.3 m pair, the points of intersection with the τ axis are denoted by L and M; these points are used for fixing τ_m with adequate resolution.

typical cross correlation functions are displayed in Fig. 11. The lag τ_m corresponding to the maximum in each cross correlation function was noted. Although the resolution of the original series was one hour, τ_m was estimated to within 0.1 h by using the differences of the zero intercepts of the main lobe marked L and M in Fig. 11. The results of this cross correlation analysis are recorded in Table 2. The positive τ_m signifies that the second (deeper) current in each pair leads the first (shallower) one, signifying an *upward* propagation of phase. The fact that no pair with a "wrong" sign of τ_m was found makes the suggestion of upward phase propagation quite plausible. The vertical phase speed $c=$ (separation)$/\tau_m$ for each pair is also recorded in Table 2. More will be said regarding the vertical propagation in the next section.

An upward phase propagation requires a downward propagation of energy, which would require that the peaks of the envelopes in Fig. 10 should shift to the right as one goes deeper. From an estimated group velocity of 0.03 cm s^{-1}, the envelope peaks should shift by 10 h in a vertical distance of 10 m. Such a shift of peaks is difficult to detect in Fig. 10 because of peak smearing, but traces of such behavior can be found, for example, between 3.4 and 40.4 m on about 1 August; between 3.4 and 14.3 m on about 17 August; between 60.6 and 80.8 m on about 7 August, etc.

As an aside, note that the 18.3 m–20.2 m pair shows a correlation of about 0.9, and from Table 1 that the rms magnitudes of the two currents had similar values. Since the 18.3 m current was measured from a surface mooring and the 20.2 m current from a subsurface mooring, it follows that the mooring motions did not contribute to any significant energy in the inertial frequency range. This agrees with the findings of Halpern *et al.* (1974b) based on current measurements during the previous year; they found disagreement only at frequencies greater than 0.4 cph.

9. Vertical turning

It has been pointed out in Section 3 that for all internal waves having a vertical propagation of phase the horizontal velocity vector at any given time turns with depth. No direct calculation of this turning exists to the knowledge of the author, although Leaman and Sanford (1975) arrived at a conclusion of turning from computation of rotary wavenumber spectra. Van Leer and Rooth (1975) observed a spiral distortion of vertical dye streaks due to higher frequency internal waves. The rate of turning can be found from (3.13) and (3.14), which give

$$\tan\phi=\frac{v}{u}=\frac{\omega}{f}\tan\left(\pm\int^z m\,dz\right), \tag{9.1}$$

where ϕ is the angle made by the horizontal velocity vector with the direction of horizontal propagation (x axis). Using $\omega\approx f$, we get

$$\frac{d\phi}{dz}=\pm m\frac{\omega}{f}\left[1+\tan^2\left(\pm\int^z m\,dz\right)\right]\Big/\left[1+\frac{\omega^2}{f^2}\tan^2\left(\pm\int^z m\,dz\right)\right]\approx\pm m(z). \tag{9.2}$$

Eq. (9.2) makes sense, since the velocity vector should turn by 360° in a distance equal to the vertical wavelength.

The band-pass filtered horizontal currents will now be used to determine if there is a consistent turning with depth. An accurate measure of the average angle between two velocity vectors is provided by the phase angle of their complex correlation coefficient (Kundu, 1976),

$$\rho=\frac{\overline{\mathbf{w}_1^*(t)\mathbf{w}_2(t)}}{[\overline{\mathbf{w}_1^*(t)\mathbf{w}_1(t)}]^{\frac{1}{2}}[\overline{\mathbf{w}_2^*(t)\mathbf{w}_2(t)}]^{\frac{1}{2}}}, \tag{9.3}$$

where $\mathbf{w}=u+iv$, the asterisk indicates complex conjugation, and subscripts 1 and 2 refer to the two stations. The quantity ρ, which is independent of the choice of the coordinate system, is a complex number whose magnitude (<1) gives the overall measure of correlation and whose phase angle gives the average counterclockwise angle of the second vector with respect to the first, the averaging process being weighted according to the magnitude of the instantaneous vectors.

The phase and magnitude of ρ for various pairs of currents are recorded in Table 2. The negative phase

TABLE 2. Results of cross correlation analysis. A positive τ_m means that the second current of the pair *leads* the first. A negative phase angle of the complex correlation coefficient ρ means that the second current is turned clockwise (looking down) of the first.

Current pair (depths in meters)	Separation (m)	Lagged correlation of u			Complex correlation of velocity vectors		
		τ_m (h)	R_{max}	c (cm s^{-1})	Phase (deg)	Magnitude	c (cm s^{-1})
3.4– 7.7	4.3	0.6	0.72	0.20	−13	0.71	0.21
3.4– 9.9	6.5	0.6	0.54	0.30	−14	0.51	0.30
3.4–14.3	10.9	2.5	0.30	0.12	−50	0.25	0.14
3.4–16.3	12.9	2.4	0.32	0.15	−59	0.27	0.14
3.4–18.3	14.9	3.3	0.42	0.13	−75	0.36	0.13
7.7– 9.9	2.2	0.0	0.92	∞	−3	0.93	0.47
7.7–14.3	6.6	0.4	0.64	0.37	−10	0.67	0.42
7.7–16.3	8.6	0.6	0.63	0.40	−14	0.59	0.39
7.7–18.3	10.6	1.2	0.61	0.25	−27	0.59	0.25
9.9–14.3	4.4	0.2	0.84	0.61	−5	0.85	0.56
9.9–16.3	6.4	0.3	0.81	0.59	−7	0.75	0.59
9.9–18.3	8.4	0.7	0.72	0.33	−17	0.70	0.32
14.3–16.3	2.0	0.0	0.97	∞	0	0.95	∞
14.3–18.3	4.0	0.2	0.91	0.56	−4	0.90	0.64
16.3–18.2	2.0	0.2	0.94	0.28	−4	0.93	0.32
18.3–20.2	1.9	0.0	0.89	∞	0	0.88	∞
20.2–40.4	20.2	6.4	0.27	0.09	−141	0.27	0.09
40.4–60.6	20.2	4.5	0.44	0.12	−115	0.51	0.11
60.6–80.8	20.2	1.2	0.42	0.47	−23	0.47	0.56
80.8–95.9	15.1	1.7	0.64	0.25	−44	0.58	0.22

angle corresponds to a clockwise turning of the current with depth, that is, an upward phase propagation. The consistency is evident by the fact that no current pair showed the opposite phase angle, although two pairs (namely 14.3 m–16.3 m and 19.3 m–20.2 m) with small separation showed zero angle. The speed of propagation obtained from the rate of turning between two currents is [using (9.2)] given by $c=\omega/(\Delta\phi/\Delta z)$, which is also recorded in Table 2, using $\omega=0.064$ cph. These speeds should be regarded as a sort of average for the depth range of the pair, i.e., a local speed.

The estimates for the phase speeds for the various depth pairs range from about 0.6 to 0.1 cm s^{-1}, ignoring the two ∞'s at small separations. The estimates appear to be satisfactory even when the correlation coefficient becomes as low as 0.25–0.3, which, however, may not be insignificant because of the long length of the series.

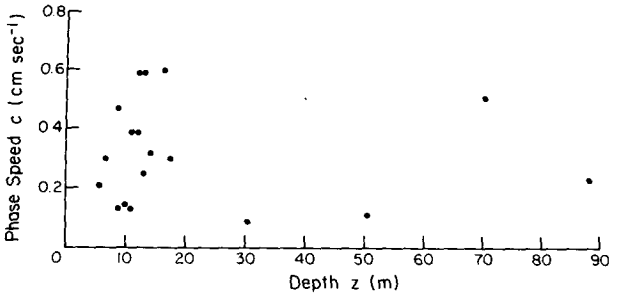

FIG. 12. Vertical phase speed versus depth. The speed is the average of those found by the two methods; the depth is taken to be the average for the pair. (Note that in this figure z is measured downward from ocean surface, whereas in Section 3 z is taken as positive upward).

Perhaps the surprising point in Table 2 is the excellent agreement of the values of c computed by the two methods.[2] The methods might at first seem to be independent of each other, since the v components are not used in the lagged correlation method, and the time delays are not used in the complex correlation method. However, this is not the case if the phase difference between u and v is nearly constant throughout each record. In any case, the agreement signifies that the values of c given are not affected much by calculation errors, but are suggested by the data themselves.

The average value of c found by the two methods is plotted against the average location of the pair in Fig. 12 (for example, for the 3.4 m–7.7 m pair, the average c of 0.205 cm s^{-1} is plotted against the average depth of $z=5.6$ m). The large scatter at small depths, which is due to the inaccuracy of the computation at small separations, makes it difficult to determine a pattern of $c(z)$ in this figure, but in general c seems to be lower at the mid-depths. This does not quite agree with the WKB relation that $m\propto N$ and therefore $c\propto N^{-1}$, which would require c to increase monotonically with depth beyond the forced layer within $z=10$ m.

The results of the cross correlation analysis are also shown in Fig. 13, where the points belonging to depths greater than 20 m are labeled in order to emphasize their relationship with other points. The slopes of lines representing the average behavior are $c=0.2$ cm s^{-1} and

[2] Since the method of calculation of the turning by determining the phase angle of the complex correlation coefficient is much easier (less expensive and requiring no interpolations to fix τ_m with adequate resolution) than the lagged correlation method, the value of the former method is apparent.

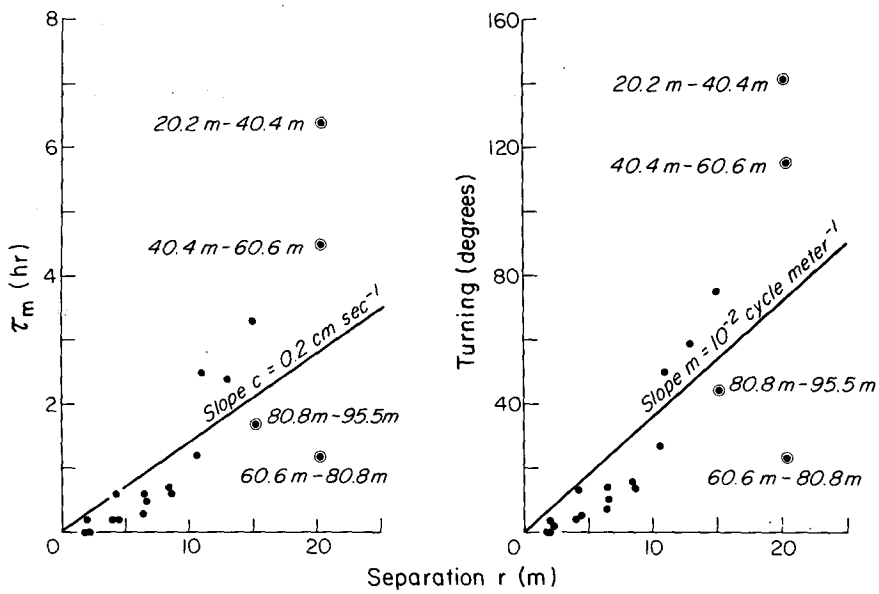

FIG. 13. (a) Lag time for maximum correlation of u components versus distance of separation. The pairs below 20 m depth are labeled. The line of slope 0.2 cm s^{-1} is indicated. (b) Phase angle of complex correlation coefficient versus distance of separation. The phase angle gives the average angular displacement (turning) between the two currents. The pairs below 20 m depth are labeled. The line of slope 10^{-2} cycle m^{-1} is indicated.

$m=10^{-2}$ cycle per meter, which are consistent with the relation $c=\omega/m$. However, the mid-depth behavior, given by the current pairs 20.2 m–40.4 m and 40.4 m–60.6 m, is more like $c=0.1$ cm s^{-1} and $m=2\times10^{-2}$ cycle per meter, which would agree with the results of Johnson *et al.* (1976).

10. Estimates of some parameters

Some parameters of the wave field will not be estimated, using the formulas resulting from the WKB approximation. Without considering depth-dependence, we shall use a typical N to be 15 cph, $\omega=0.064$ cph, $f=0.0592$ cph, $c=\omega/m=0.2$ cm s^{-1}, and Eqs. (3.9) and (3.16). The following values are then obtained:

$$\left.\begin{aligned} &m\approx 9\times10^{-3} \text{ cycle per meter}\\ &k_H=(k^2+l^2)^{\frac{1}{2}}\approx 1.5\times10^{-5} \text{ cycle per meter}\\ &\lambda_z=\frac{1}{m}\approx 110 \text{ m}\\ &\lambda_H=\frac{1}{k_H}\approx 60 \text{ km}\\ &c_g\approx 0.03 \text{ cm s}^{-1} \end{aligned}\right\}.$$

The ratio (potential plus vertical kinetic energy)/(horizontal kinetic energy) for internal waves is, from Fofonoff (1969), given by

$$(N^2+\omega^2)(\omega^2-f^2)/(N^2-\omega^2)(\omega^2+f^2) \approx(\omega^2-f^2)/(\omega^2+f^2)\approx 0.077$$

for $\omega=1.08f$. The energy density is therefore $E=1.077\rho_2^1|\mathbf{V}|^2$. Near the bottom, a typical maximum inertial $|\mathbf{V}|$ may be taken to be about 10 cm s^{-1}, giving a typical maximum $E\approx 50$ erg cm^{-3}. The downward inertial energy flux, when inertial "bursts" occur, is therefore $F=Ec_g\approx 1.5$ erg cm^{-2} s^{-1}. For comparison, the rate of turbulence production in the bottom boundary layer due to the work done by the exterior ("geostrophic") velocity $\mathbf{V}_g$ against the bottom stress τ_B is $V_g\tau_B$. At the current meter station, representative values are $V_g\approx 10$ cm s^{-1} and $\tau_B\approx 0.2$ dyn cm^{-2} (Kundu, 1976; Caldwell, 1976) corresponding to a drag coefficient of 0.002, giving a turbulence production rate of 2 erg cm^{-2} s^{-1}. The order of magnitude agreement signifies that inertial events, when they occur, can significantly stir the boundary layer.

Using the expression $\tan^{-1}(k_H/m)$, the inclination of the phase velocity vector with the vertical (which is also equal to the inclination of the group velocity vector with horizontal) is estimated to be 0.1°. From the bathymetric contours of Fig. 1, it appears that the slope of the ocean bottom near the current meter station was fairly uniform. The bottom slope is estimated to be about 0.4°, from the observation that the horizontal separation between the 150 and 50 m contours is about 14 km. Since this slope is larger than the estimated slope of the characteristic, a wave packet propagating landward and downward would be reflected back into the ocean, to travel seaward and downward (see Fig. 2.10 of Turner, 1973). Only the upper current meters at the station could be affected by the rays originating in the surface layer inshore of the

station and propagating downward and seaward. These conclusions, however, may not be realistic, since the depth dependence of $N(z)$ has not been considered in these estimates (see Fig. 12 of Hayes and Halpern, 1976).

However, whether the energy really gets reflected off the sea bed, or gets absorbed by the dissipation in the turbulent bottom boundary layer, is not a trivial matter to decide, and we shall not attempt to do it here. Apparently, the rate of viscous dissipation per unit volume of the bottom boundary layer (ϵ) adjusts in response to an oncoming flux of energy into the boundary layer. If ϵ can be large enough, no reflection should result.

Most of the inertial energy, presumably, could be traced back to the upper wind-mixed layer of the ocean. Following Niiler (1975), the vertical flux of energy at the ocean surface due to the wind input, minus the amount used in dissipation in the mixed layer, is given by $m_0|\tau/\rho|^{\frac{3}{2}}$, where m_0 is an O(1) quantity and τ is the wind stress. For a typical wind event of $\tau=3$ dyn cm^{-2}, this flux is about 5 erg cm^{-2} s^{-1}, which is somewhat larger but of the same order as our estimate of the vertical inertial energy flux within the water column. Acting over a period of time such inertial energy fluxes, therefore, can cause appreciable draining of the mixed layer.

From (3.10)–(3.12), the ratio of the amplitudes of the vertical and horizontal velocities is $\hat{w}/\hat{u}_H=k_H/m$. For a maximum horizontal amplitude of 20 cm s^{-1}, this gives $\hat{w}\approx 0.03$ cm s^{-1}. The corresponding maximum vertical displacement would be $\hat{\xi}=\hat{w}/\omega\approx 3$ m, which may be measurable by "pycnocline followers" (Rooth and Düing, 1971).

It is of interest to estimate the effect of large-scale deformation of the mean flow field according to (3.16). The maximum horizontal shear $\bar{v}_x$ was of order 10^{-5} s^{-1} in the region of the experiment (see Fig. 3 of Kundu and Allen, 1976), so that the term $f\bar{v}_x$ appears to be an order of magnitude smaller than f^2. From hydrographic measurements during this experiment (Fig. 2 of Kundu *et al.*, 1975), the slope of the isopycnals during an upwelling event appears to be about 1/250, giving $s^2N^2\sim 10^{-8}$ s^{-2}, which is of the same order as f^2. Thus, appreciable variations of passband and all parameters except frequency are possible due to this effect.

11. Summary and discussion

The current meter data at eleven depths at a station off the coast of Oregon in 100 m of water have been analyzed. The average spectra showed about an 8% increase in the frequency of the "inertial" peak ($\omega\approx 0.064$ cph; period ≈ 15.6 h) above the local f ($=0.0592$ cph; period ≈ 16.9 h). The spectra also show a smaller secondary peak at 2% below f. A closer analysis of the behavior of the inertial motion versus time showed that, while the dominant behavior was an increase of frequency above f, some individual events indeed had frequencies close to but slightly less than f, which may be due to the mean horizontal density gradients or the Doppler effect.

The amplitude of inertial oscillations decays slowly with depth; at a depth of 80 m their magnitudes are about half those found in the surface layer. This conflicts with the model of Pollard (1970), and the conclusion of Hayes and Halpern (1976) using the same data as ours, that the inertial energy decays rapidly below the mixed layer. The decrease of the inertial amplitudes with depth between 10 and 80 m was in qualitative agreement with that given by the WKB solution, namely u, $v\sim N^{\frac{1}{2}}$. There seems to be a rapid decay very near the bottom (within about 10 m).

Because of the close proximity of the diurnal and semidiurnal tidal periods on the two sides of the inertial period, a sharp bandpass filter centered at $\omega=0.064$ cph was used to isolate the inertial motions. This sharp filtering necessarily resulted in the smearing of peaks in the time domain, but the phases were preserved. A lagged correlation of these inertial currents at different depths clearly showed an upward propagation of phases throughout the water column at a mean speed of $c\approx 0.2$ cm s^{-1}. The mid-depth speeds were about 0.1 cm s^{-1}, in agreement with the cyclesonde measurements of Johnson *et al.* (1976), also conducted in the neighborhood of the present experiment. Their work shows a striking example of an inertial event with phases coherently propagating upward from a depth of about 70 m to about 20 m. There is other evidence of upward phase propagation in their measurements, but in these the phases became uncorrelated in a vertical distance of about 20 m. This fact also agrees with our calculations that the correlation coefficient becomes small after a distance of separation of about 20 m.

The inertial currents were found to turn clockwise (looking down) with depth, as required for upward phase propagation, and the phase speeds implied by the rates of turning with depth agreed surprisingly well with the lagged correlation calculations. Such a direct calculation of the turning of inertial currents with depth is believed to be new.

The work of Johnson *et al.* (1976) also gives a clear demonstration of the downward propagation of the wave groups at a speed of about $c_g\approx 0.03$ cm s^{-1}. The propagation of wave groups is difficult to detect in our results due to peak smearing, but traces of it have been found. An estimate of c_g using a WKB formula gives $c_g\approx 0.03$ cm s^{-1}.

The downward flux of inertial energy near the bottom during a typical large inertial burst is estimated to be about 1.5 erg cm^{-2} s^{-1}. The rate of turbulence production within the bottom boundary layer due to the "mean" geostrophic flow is estimated to be 2 erg cm^{-2} s^{-1}. The order of magnitude agreement suggests that such fluxes do stir up the boundary layer.

The downward flux of energy from the upper mixed layer is estimated to be about 5 erg cm^{-1} s^{-1}, so that the inertial energy flux can be a large fraction of the mixed layer draining.

The apparent vertical propagation does not support the concept of standing waves in the vertical. An equivalent mode number, however, can be defined as the depth of water divided by half the vertical wavelength. Vertical phase speeds of 0.1–0.4 cm s^{-1} require vertical wavelengths of 55 m–225 m, which for an ocean depth of 100 m would suggest mode number of around 1–4. Perkins (1972) found some evidence of a standing third mode in the Mediterranean Sea ($\sim$1500 m deep). The open ocean ($\sim$5500 m deep) measurements of Sanford (1975), however, suggest a higher order vertical structure.

The time-averaged hodograph of the horizontal velocity vector of the inertial currents have been found to be clockwise ellipses of axis ratio 1.03–1.28. Theoretically, with an 8% increase in frequency above f, the ratio should be 1.08. A majority of these ellipses have their major axes aligned roughly east-west, signifying a horizontal propagation perpendicular to the coast. The horizontal wavelength is estimated to be 60 km. This is in fair agreement with the measurement of Webster (1968) who gave a phase difference of 34° (coherence 0.7) between two stations separated by 3 km east-west, signifying a wavelength of about 32 km. Schott (1971) also estimated the horizontal wavelength to be about 50 km.

Some similarities are detected between the observed inertial currents in the surface layer and that computed from the simple wind-forced model of Pollard and Millard (1970). However, at least one example of a large inertial amplitude in the surface layer not related to any wind event has also been noted. Apparently the phenomena near the present coastal region cannot be completely described by their very simple model. In any case, even a qualitative success of such a simple theory is gratifying.

In this connection, we would like to draw attention to a remark of Pollard (1970) concerning the observed intermittency of inertial oscillations. He finds that the transient behavior and rapid decay rates cannot be explained by a dispersion of inertial oscillations out of a forced region, and concludes (Pollard, 1970; Pollard and Millard, 1970) that the destruction of inertial oscillations must be due to a second wind stress running against the existing inertial oscillations in the surface layer. The argument was later supported by Smith (1973). The present author feels that, while there is some truth to the fact that the wind can decrease the amplitude of an existing inertial oscillations by running against its phase, this fact cannot be solely responsible for the observed intermittency. Moreover, if that were true then one would not need the term $-c\mathbf{u}$ in the Pollard-Millard model. Hasselman (1970) explains the intermittency as due to the phase mixing of modes with closely nieghboring frequencies, produced by various possible mechanisms like the horizontal inhomogeneity of the oceanic properties (N, f, water depth) and of the driving field, the horizontal component of the Coriolis force, nonlinear interactions with the low frequency "mean" currents, etc.

Finally, some of the estimates in this study based on the WKB formulas and a depth-independent N (= 15 cph) may be questionable. Not only can this scheme be invalid in the region because the scales of variation of the ocean properties are not larger than the scale of the wave field, but also because *all* of the inertial energy has been considered to be shifted 8% above the local f, the vertical propagation being held solely responsible for this shift. However, the agreement between our estimate of c_g with that of Johnson *et al.* (1976) renders some credibility to our calculations.

Acknowledgments. This research was supported by the Coastal Upwelling Ecosystems Analysis Program (CUEA) of the International Decade of Ocean Exploration Office (IDOE) of the National Science Foundation under Grants IDO71-04211 and OCE76-00596.

I am very grateful to Drs. David Halpern and Robert L. Smith for making their current meter data available to me and to J. S. Allen, D. R. Caldwell, J. Kroll, C. N. K. Mooers, P. P. Niiler, and R. O. R. Y. Thompson for comments on the manuscript; the extensive comments by Dr. Mooers were particularly helpful. Drs. T. B. Sanford and Jacques Nihoul both pointed out an error in an earlier version.

REFERENCES

Caldwell, D. R., 1976: Fine scale temperature structure in the bottom mixed layer on the Oregon shelf. *Deep-Sea Res.* (in press).

Day, C. G., and F. Webster, 1965: Some current measurements in the Sargasso Sea. *Deep-Sea Res.*, **12**, 805–814.

Fofonoff, N. P., 1969: Spectral characteristics of internal waves in the ocean. *Deep-Sea Res.*, **16**, 58–71.

Fomin, L. M., 1973: Inertial oscillations in a horizontally inhomogeneous current velocity field. *Izv. Atmos. Oceanic Phys.*, **9**, 37–40.

——, and M. T. Savin, 1973: Vertical coherence of inertial motions in the ocean. *Izv. Atmos. Oceanic Phys.*, **9**, 182–183.

Frankignoul, C. J., 1974: Preliminary observations of internal wave energy flux in frequency depth space. *Deep-Sea Res.*, **21**, 895–909.

Gonella, J., 1971: A local study of inertial oscillations in the upper layers of the ocean. *Deep-Sea Res.*, **18**, 775–788.

Halpern, D., 1974: Observations of the deepening of the wind-mixed layer in the Northeast Pacific Ocean. *J. Phys. Oceanogr.*, **4**, 454–466.

——, 1976: Structure of a coastal upwelling event observed off Oregon during July 1973. *Deep-Sea Res.*, **23**, 495–508.

——, J. R. Holbrook and R. M. Reynolds, 1974a: A compilation of wind, current and temperature measurements: Oregon, July and August 1973. CUEA Technical Report 6, Ref. M74–73. Dept. of Oceanography, University of Washington, 190 pp.

——, R. D. Pillsbury and R. L. Smith, 1974b: An intercomparison of three current meters operated in shallow water. *Deep-Sea Res.*, **21**, 489–497.

Hasselman, K., 1970: Wave-driven inertial oscillations. *Geophys. Fluid Dyn.*, **1**, 463–502.

Hayes, S. P., and D. Halpern, 1976: Observations of internal waves and coastal upwelling off the Oregon coast. *J. Mar. Res.*, **34**, 247–267.

Johnson, W. R., J. C. Van Leer and C. N. K. Mooers, 1976: A cyclesonde view of coastal upwelling. *J. Phys. Oceanogr.*, **6**, 556–574.

Kroll, J., 1975: The propagation of wind-generated inertial oscillations from the surface into the deep ocean. *J. Mar. Res.*, **31**, 15–51.

Kundu, P. K., 1976: Ekman veering observed near the ocean bottom. *J. Phys. Oceanogr.*, **6**, 238–242.

——, J. S. Allen and R. L. Smith, 1975: Modal decomposition of the velocity field near the Oregon coast. *J. Phys. Oceanogr.*, **5**, 683–704.

——, and J. S. Allen, 1976: Some three-dimensional characteristics of low-frequency current fluctuations near the Oregon coast. *J. Phys. Oceanogr.*, **6**, 181–199.

Leaman, K. D., 1975: The vertical propagation of inertial waves in the ocean. Ph.D. thesis, MIT-Woods Hole, 174 pp.

——, and T. B. Sanford, 1975: Vertical energy propagation of inertial waves: A vector spectral analysis of velocity profiles. *J. Geophys. Res.*, **80**, 1975–1978.

Mooers, C. N. K., 1975: Several effects of a baroclinic current on the cross-stream propagation of internal-inertial waves. *Geophys. Fluid Dyn.*, **6**, 242–275.

Munk, W., and N. Phillips, 1968: Coherence and band structure of inertial motion in the sea. *Rev. Geophys.*, **6**, 447–471.

Nayfeh, A. H., 1973: *Perturbation Methods*. John Wiley.

Niiler, P. P., 1975: Deepening of the wind-mixed layer. *J. Mar. Res.*, **33**, 405–422.

Perkins, H., 1970: Inertial oscillations in the Mediterranean. Ph.D. thesis, MIT-Woods Hole, 155 pp.

——, 1972: Inertial oscillations in the Mediterranean. *Deep-Sea Res.*, **19**, 289–296.

Pillsbury, R. D., J. S. Bottero, R. E. Still and W. E. Gilbert 1974: A compilation of observations from moored current meters, Vol. VII, Oregon Continental Shelf, July–August 1973. IDOE Data Report 58, Ref. 75-7, 87 pp.

Pollard, R. T., 1970: On the generation by winds of inertial oscillations in the ocean. *Deep-Sea Res.*, **17**, 795–812.

——, and R. C. Millard, 1970: Comparison between observed and simulated wind-generated inertial oscillations. *Deep-Sea Res.*, **17**, 813–821.

Rooth, C., and W. Düing, 1971: On the detection of inertial waves with pycnocline followers. *J. Phys. Oceanogr.*, **1**, 12–16.

Sanford, T. B., 1975: Observations of the vertical structure of internal waves. *J. Geophys. Res.* **80**, 3861–3871.

Schott, F., 1971: Spatial structure of inertial-period motions in a two-layered sea, based on observations. *J. Mar. Res.*, **29**, 85–102.

Smith, R., 1973: Evolution of inertial frequency oscillations. *J. Fluid Mech.*, **60**, 383–389.

Tomczak, M., 1968: Über interne Wellen in der Nähe der Trägheitsperiode. *Deut. Hydrogr. Z.*, **21**, 145–151.

Turner, J. S., 1973: *Buoyancy Effects in Fluids*. Cambridge University Press, 367 pp.

Van Leer, J. C., and C. G. Rooth, 1975: Shear observations in the deep thermocline. *Deep-Sea Res.*, **22**, 831–836.

Webster, F., 1968: Observations of inertial-period motions in the deep sea. *Rev. Geophys..*, **6**, 473–490.